Enhanced Radio-Frequency Field Penetration in an Inductively Coupled Plasma

M. Tuszewski (P-24)

The multibillion-dollar semiconductor industry uses plasma processing to produce various components, including multiple wafers, multichip modules, and flat panel displays. Always searching for methods that will increase yield and throughput and that, at the same time, will allow them to make smaller components, semiconductor manufacturers are focusing much effort on developing uniform, high-density, large-area plasmas that will help them optimize techniques such as sputtering, etching, and ion implantation and deposition. As part of this effort, Los Alamos has worked with Novellus Systems, a leading U.S. manufacturer of semiconductor process equipment, to develop and study a low-frequency, inductively coupled plasma (ICP) source for producing semiconductor devices with 0.25-μm geometries.

ICPs consist of a dielectric chamber surrounded by a conducting coil. Radio-frequency (rf) power is continuously applied to the coil and induces electric fields that partially ionize a gas inside the chamber and sustain a discharge. Most of the rf power is absorbed by the plasma; understanding this absorption is necessary for describing ICP heating and transport properties, which are important factors in predicting whether a plasma is radially uniform. Present models that consider induced rf electric fields (but not magnetic fields) predict that the rf power transfers to plasma electrons within a thin skin layer near the plasma surface. For typical rf frequencies of 0.1–13.56 MHz, the skin depths δ are a few centimeters, whereas the device dimensions are 10–30 cm.

During our work with Novellus, we obtained data that contradicted the current models by indicating deep rf penetration into argon ICP discharges with small skin depths. Because such deep penetrations are needed in semiconductor manufacturing processes,

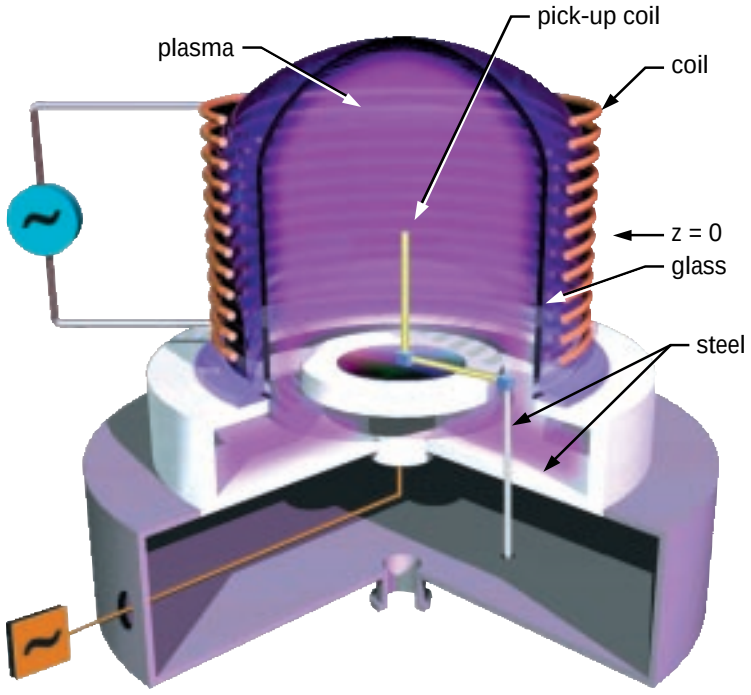

Fig. II-33. Sketch of the inductively coupled plasma.

this enhanced rf field penetration—previously unknown to the semiconductor manufacturers—was an important breakthrough. We realized that we would have to invoke a new mechanism to explain the enhanced penetration. Fluid calculations suggested that this mechanism is a reduction of the plasma conductivity by the induced rf magnetic fields when the electron cyclotron angular frequency ω_c exceeds both the rf angular frequency ω and the electron-neutral collision frequency ν, a condition that is satisfied for many low-pressure ICPs. Hence, the induced rf magnetic fields must be included in ICP models to predict electron heating and the resulting plasma transport.

To test this mechanism experimentally, we measured the induced rf magnetic fields inside a cylindrical ICP, which is sketched in Fig. II-33. A 13-turn copper coil was wound around a glass bell jar with an inner radius of 16.5 cm, and the coil was powered by a 2-kW, 0.46-MHz (ω = 2.9 megacycle) rf generator. A small pick-up coil (with 18 turns, a diameter of 4 mm, and a length of 5 mm) with shielded, twisted leads was inserted near the closed end of a 6-mm-diameter ceramic tubing, which was connected to a stainless-steel shaft via ceramic transition pieces. We oriented the pick-up coil to measure the z (upward) component of the induced rf magnetic field, and we obtained radial scans in the coil midplane (z = 0) by rotating the steel shaft.

Argon discharges were sustained with gas pressures of 5–50 mtorr and with rf powers of 0.5–1.5 kW. We obtained radial profiles of the ion density (Fig. II-34) and estimates of the electron temperatures T_e from a voltage-swept, cylindrical Langmuir probe. For the discharges of Fig. II-34, the T_e profiles are radially uniform, and the electron energy distributions are almost Maxwellian. We also calculated the collision frequency to within 10% of the collision frequencies used in other ICP experiments and models. Our measured magnitudes $|B|$ of the induced rf magnetic field B_z are shown with symbols in Fig. II-35 for 5-mtorr argon discharges. The $|B|$ profiles are quite flat near the wall and change curvature at smaller radii. The magnitudes of B and of the coil azimuthal electric field E_c increase with rf power.

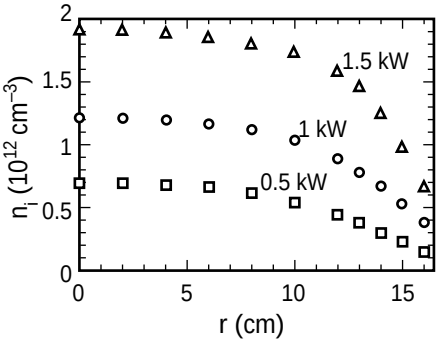

Fig. II-34. Measured radial profiles of the ion density for argon discharges with 5-mtorr gas pressure and with 0.5-, 1-, and 1.5-kW rf power.

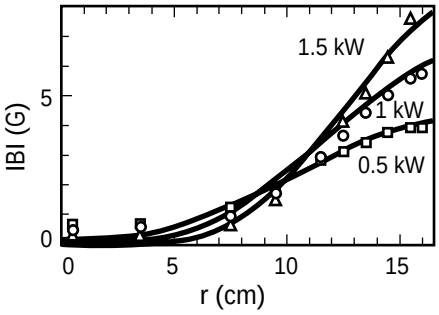

Fig. II-35. Radial profiles of the rf magnetic-field amplitude for 5-mtorr argon discharges. The measured data are indicated with symbols, and the magnetized calculations are shown with solid lines.

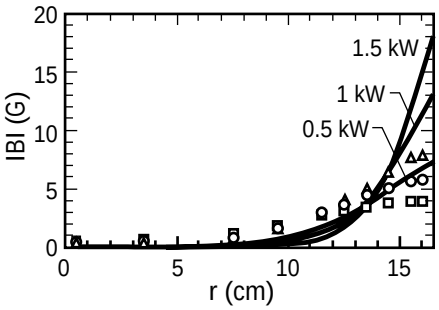

Fig. II-36. Radial profiles of the rf magnetic-field amplitude for 5-mtorr argon discharges. The measured data are indicated with symbols, and the unmagnetized calculations are shown with solid lines.

We first compared our magnetic-field data with the predictions from existing models by using a fluid approach to describe the ICP discharges. For simplicity, we used a one-dimensional model with $B = B_z(r)$, where r is the radius of the ICP. Combining Faraday's, Ohm's, and Ampere's laws, we obtained the following expression:

$$(1/r)(d/dr)(r/\sigma)(dB/dr) = i\omega\mu_0 B \ , \qquad (1)$$

where $\sigma = ne^2/[m(\nu + i\omega)]$ is the plasma conductivity, n is the plasma ion density, m is the electron mass, and μ_0 is the permeability of free space. We solved this equation with the density profiles of Fig. II-34.

The calculated radial $|B|$ profiles are shown in Fig. II-36 with solid curves, and the experimental data are also shown with symbols for comparison. The calculated $|B|$ magnitudes and decays are overestimated by factors of 2–3. In addition, the exponential-like calculated profiles do not reproduce the change of curvature observed near the wall. The uncertainties in the calculated penetration depths δ_c are estimated to be about 40%, but these uncertainties do not explain the above discrepancies. Clearly, a better model is required.

Previously, when we had calculated σ, we had neglected a magnetic term that introduces a nonlinearity into the electron momentum equation from which σ is derived. After including this magnetic term, we were able to define the following effective conductivity $\langle\sigma\rangle$ that is time averaged over an rf period:

$$\langle\sigma\rangle = \sigma_0/(1+|\omega_c|^2/\nu^2)^{1/2} - i\sigma_0(\omega/\nu)/(1+|\omega_c|^2/\nu^2)^{3/2} \ , \quad (2)$$

where $\sigma_0 = ne^2/(m\nu)$ is the zero-frequency collisional conductivity. Replacing σ with the value of $\langle\sigma\rangle$, we solved Eq. 1 again. The calculated $|B|$ profiles are shown in Fig. II-35 with solid curves. The calculated and observed $|B|$ magnitudes agree within 5% near the wall, and the calculations also reproduce the shape of the observed profiles. The edge flattening and the change in the profile curvature are due to low edge plasma conductivities $\langle\sigma\rangle$.

We also measured the $|B|$ profiles for argon discharges with higher gas pressures of 10–50 mtorr. The magnetized calculation agrees with the data for all pressures, and the discrepancy between the unmagnetized calculation and the data gradually diminishes as the gas pressure increases. The experimental data and both

calculations coincide within the uncertainties for 40- and 50-mtorr discharges. This agreement is expected since $\langle\sigma\rangle \approx \sigma$ in high-pressure discharges for which ν exceeds $|\omega_c|$ through most of the plasma volume. The agreement between the data and the calculations also implies that the combined experimental uncertainties are less than a factor of 2.

In addition to studying argon discharges, we also measured and calculated the $|B|$ profiles of oxygen discharges, which are more representative of industrial ICPs. These oxygen discharges yield results that are qualitatively similar to those for argon, except that the rf penetration depths are larger by factors of 2–3 because the oxygen discharges have lower plasma densities. The rf magnetic fields of the oxygen discharges are 1–3 G on the axis. Hence, the plasma conductivity is substantially reduced by the rf magnetic field at all radii.

Although we did not experimentally investigate cases with $|\omega_c| > \omega > \nu$, numerical averages of σ over an rf period suggest that Eq. 2 remains a good approximation whenever $|\omega_c|$ is greater than ω and ν, regardless of the relative magnitudes of ω and ν. Hence, the ICP rf-power absorption depends on the largest of ω, ν, $|\omega_c|$, and the effective stochastic frequency ν_s. The regime where $|\omega_c|$ is the largest has been overlooked until now. Because the induced rf magnetic fields are only 3–10 G for typical rf powers (seemingly negligible), they are usually neglected in ICP models. However, the corresponding values of $|\omega_c| \approx (50\text{–}180) \times 10^6$ rad/s are often larger than typical values of $\nu \approx (5\text{–}20) \times 10^6$ s^{-1} and $\omega \approx (1\text{–}85) \times 10^6$ rad/s. As a result, the rf penetration depths δ are often substantially increased by the rf magnetic field, and the ohmic heating-power densities ($\sim 1/\delta^2$) can be reduced by an order of magnitude.

In summary, the induced rf magnetic fields of a low-frequency ICP show substantial penetration, whereas existing models predict absorption in a thin skin layer. Fluid calculations resolve this apparent contradiction: the induced rf magnetic fields appreciably reduce the plasma conductivity, which leads to a larger rf penetration. The rf magnetic fields can significantly modify the electron heating and the resulting plasma transport in many of today's low-pressure ICPs, and they should therefore be included in future ICP models.